

Safety-Critical Formation Control of Non-Holonomic Multi-Robot Systems in Communication-Limited Environments

Vishrut Bohara and Siavash Farzan

Abstract—This paper introduces a decentralized estimator-based safety-critical controller designed for formation control of non-holonomic mobile robots operating in communication-constrained environments. The proposed framework integrates a robust state estimator capable of accurately reconstructing neighboring agents' velocity vectors and orientations under varying dynamic conditions, with a decentralized formation tracking controller that leverages Control Barrier Functions (CBFs) to guarantee collision avoidance and inter-agent safety. We present a closed-form control law that ensures both stability and string stability, effectively attenuating disturbances propagating from leader to followers. The theoretical foundations of the estimator and controller are established using Lyapunov stability analysis, which confirms global asymptotic stability under constant velocities and global uniformly ultimate boundedness under time-varying conditions. Extensive numerical simulations and realistic Gazebo-based experiments validate the effectiveness, robustness, and practical applicability of the proposed method, demonstrating precise formation tracking, stringent safety maintenance, and disturbance resilience without relying on inter-robot communication.

I. INTRODUCTION

Multi-robot systems and connected autonomous vehicles have emerged as pivotal technologies, significantly enhancing productivity, scalability, and operational efficiency across various domains such as environmental monitoring, industrial automation, urban traffic management, and disaster response [1]. Formation control—the ability of multiple agents to maintain spatial configurations during cooperative tasks—is fundamental for platooning and coordinated multi-vehicle maneuvers. In safety-critical scenarios, such as search-and-rescue operations, cooperative adaptive cruise control, and tasks within communication-jammed environments, achieving robust, collision-free, and stable formation control under limited V2V/V2I bandwidth is paramount. However, these environments often impose stringent constraints on communication reliability and introduce significant sensor uncertainty, posing substantial challenges to conventional formation control methods.

Numerous formation control schemes have been proposed to tackle challenges related to stability, robustness, and communication constraints [2]. Observer-based controllers have been successfully utilized to maintain formations in quadrotor systems under uncertain velocities and disturbances [3]. Other approaches leverage trajectory estimation techniques, such

as Extended Kalman Filters, to realize formation control without explicit inter-agent communication [4]. However, these strategies often lack theoretical guarantees for stability and robustness, particularly under strict communication limitations. The formation control method presented in [5], although capable of handling limited communication through distributed estimation, does not address entirely communication-free scenarios. Similarly, methods employing bearing-based estimation and orientation-independent strategies [6], [7] have advanced the state-of-the-art but still fall short in comprehensively addressing safety-critical constraints in communication-deprived environments.

Recent advances in Control Barrier Functions (CBFs) [8] have demonstrated significant promise for ensuring inter-agent and environmental safety in multi-robot systems. For instance, high-order CBFs have been integrated into formation control frameworks to guarantee safety under the assumption of local communication availability [9]. Additionally, displacement-based formation control approaches that utilize artificial potential fields combined with CBFs have shown effectiveness in collision avoidance, yet often lack rigorous stability analyses and validation in physically realistic environments [10]. Further integration of CBFs with reinforcement learning [11] and model predictive control frameworks [12] has extended the applicability of safety-critical controls, though the emphasis remains limited in terms of comprehensive theoretical guarantees and realistic validation for non-holonomic robotic platforms.

Furthermore, formation reconfiguration and obstacle avoidance studies, such as those presented in [13], [14], effectively demonstrate adaptability in heterogeneous robot swarms but typically overlook explicit safety and stability guarantees in communication-restricted conditions. The authors of [15] propose a unified framework using CBF and Lyapunov functions for safety and stability but do not address communication constraints or realistic validation. Other notable approaches leveraging distributed observers and state estimation to achieve leader-follower formation control without explicit communication have been explored [16], [17], [18]. Nevertheless, these approaches have not provided comprehensive closed-form solutions or unified frameworks combining estimation-based state reconstruction, robust safety enforcement, and stability guarantees applicable explicitly to non-holonomic multi-robot systems. A related study in [19] utilizes an estimator-based controller to achieve safety and stability in adaptive cruise control, which can be seen as a simplified one-dimensional formation control scenario.

Vishrut Bohara is with the Robotics Engineering Department, Worcester Polytechnic Institute, Worcester, MA 01609, USA (e-mail: vbohara@wpi.edu)

Siavash Farzan is with the Electrical Engineering Department, California Polytechnic State University, San Luis Obispo, CA 93407, USA (e-mail: sfarzan@calpoly.edu)

To bridge these research gaps, we propose a fully decentralized safety-critical formation control framework for non-holonomic multi-robot systems operating entirely without inter-agent communication. Our approach uniquely integrates a robust state estimator into an analytical control law using CBFs, avoiding the computational overhead of online optimizations while strictly ensuring collision avoidance and maintaining formation integrity in severely communication-constrained scenarios. The main contributions are:

- i. Development of a novel, robust estimator explicitly tailored for non-holonomic robotic agents, providing global asymptotic stability under constant velocities and global uniformly ultimate boundedness under time-varying velocities.
- ii. Derivation of explicit safety-critical control bounds via Control Barrier Functions that ensure collision-free operation without relying on any inter-agent communication or numerical optimization methods.
- iii. Formulation of a decentralized, analytical closed-form control law integrating the estimator and safety constraints, rigorously verified through Lyapunov-based stability analysis, guaranteeing stable, collision-free formation tracking.
- iv. Analytical verification of string stability within the proposed closed-form framework, ensuring attenuation of disturbances throughout the formation hierarchy, thus achieving robustness against propagating perturbations.
- v. Comprehensive validation through numerical simulations and realistic Gazebo-based experiments, demonstrating the practical applicability, computational efficiency, and robustness of the proposed closed-form approach under diverse operational conditions.

The remainder of this paper is organized as follows: Section II defines the safety-critical leader-follower formation control problem and specifies the underlying system dynamics. Section III introduces the proposed estimator-based safety-critical controller and details its mathematical formulation, stability proofs, and integration mechanisms. Section IV provides a thorough performance evaluation of the proposed method via simulations and physics-based experiments in Gazebo. Finally, Section V concludes with key insights and outlines future research directions.

II. PROBLEM DESCRIPTION

In safety-critical leader-follower formation control, a group of robots is coordinated to maintain a prescribed spatial configuration while guaranteeing collision avoidance. In environments with limited communication and potentially noisy or incomplete sensor measurements, ensuring safety and stability becomes mathematically challenging.

This work addresses a sub-problem of leader-follower formation control under the following conditions: Each robot measures its own linear velocity and the relative distances to other agents, but there is no inter-agent communication. All robots operate with non-negative linear velocities and are equipped with sensors that provide both radial and angular measurements of neighboring agents. A key requirement is that the center of rotation of the leader's trajectory lies exterior to the formation, which is necessary for achieving feasible control.

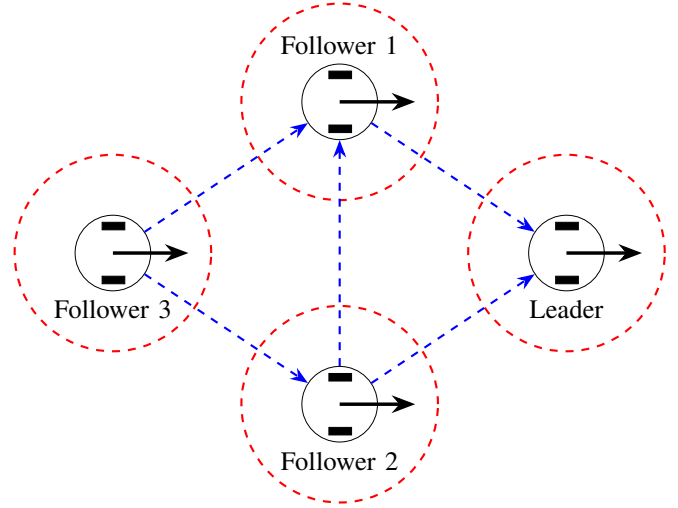


Fig. 1. Leader-Follower formation control of mobile robots in a diamond formation, illustrating inter-agent interaction edges and safety boundaries. The red dashed circles denote the safety regions for each robot, and the blue dashed arrows represent predecessor-follower interactions, where followers maintain desired distances from their predecessors without communication.

We propose a decentralized framework that integrates state estimation with safety-critical control. The framework guarantees convergence of the estimator, string stability of the formation, and inter-agent safety. Although the focus is on leader-follower architectures (one of the most safety-critical), the underlying estimator design can be generalized to broader decentralized multi-agent systems in two-dimensional settings.

A. Predecessor-Follower Dynamics

We consider the dynamics of a predecessor-follower pair in a leader-follower formation. Let the i^{th} robot (the follower) track its predecessor, the $(i-1)^{th}$ robot. In the follower's local coordinate frame (see Fig. 2), we introduce the following variables. *State Variables:* The state of the system is characterized by the Euclidean distance (d) between the follower and its predecessor, the angle (θ) between the line-of-sight (from the follower to the predecessor) and the follower's heading, the linear velocities of both the predecessor and follower (v_1 and v respectively), and the relative orientation (ψ), defined as the angle between the predecessor's heading and the follower's x -axis, i.e. follower's heading. From these states, the observable states for followers are d, θ, v .

Control Inputs: The control inputs in the dynamics are the linear accelerations of the predecessor and follower (u_1 and u , respectively), and the angular velocities of both robots (ω_1 and ω), which control the heading of the agent. The follower's control objective is to compute u and ω to track the desired inter-agent distance.

System Dynamics: The continuous-time dynamics of the pair are described by:

$$\begin{aligned} \dot{d} &= v_1 \cos(\theta - \psi) - v \cos \theta, \\ \dot{\theta} &= \frac{v \sin \theta - v_1 \sin(\theta - \psi)}{d} - \omega, \\ \dot{v}_1 &= u_1, \quad \dot{v} = u, \\ \dot{\psi} &= \omega_1 - \omega. \end{aligned} \tag{1}$$

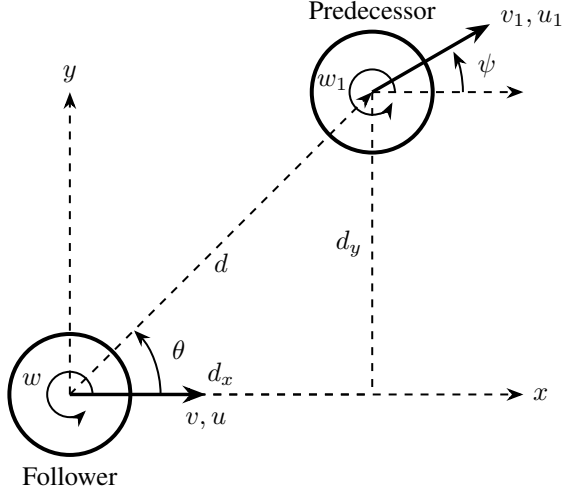


Fig. 2. Predecessor-follower pair and associated parameters in a leader-follower formation control setting.

For further analysis, we project these dynamics onto the follower's local frame by defining the coordinate transformations:

$$\begin{aligned} d_x &= d \cos \theta, & d_y &= d \sin \theta, \\ v_{1x} &= v_1 \cos \psi, & v_{1y} &= v_1 \sin \psi, \end{aligned}$$

and by introducing the projected accelerations

$$a_x = u_1 \cos \psi - v_{1y} \omega_1, \quad a_y = u_1 \sin \psi + v_{1x} \omega_1.$$

Then, the dynamics in the follower's frame become:

$$\begin{aligned} \dot{d}_x &= v_{1x} - v + d_y \omega, \\ \dot{d}_y &= v_{1y} - d_x \omega, \\ \dot{v}_{1x} &= a_x + v_{1y} \omega, \\ \dot{v}_{1y} &= a_y - v_{1x} \omega. \end{aligned} \quad (2)$$

Constraints: The system is subject to the following bounds:

$$\begin{aligned} 0 \leq v \leq v_{\max}, \quad |u| \leq u_{\max}, \quad |\omega| \leq \omega_{\max}, \\ |a_x|, |a_y| \leq u_{\max} + v_{\max} \omega_{\max} \triangleq a_{\max}. \end{aligned} \quad (3)$$

B. Formation Control

We model the formation as a directed acyclic graph (DAG) $G = (V, E)$ where the node set is

$$V = \{L, F_1, F_2, \dots, F_n\},$$

with L denoting the leader and F_i , $i = 1, \dots, n$, representing the follower agents. The directed edges in E represent the predecessor-follower relationships and are classified as follows:

i. Edge Classification:

- X^+ -edges: Along these edges, the follower maintains a velocity-dependent distance from its predecessor along its local X -axis.
- Y -edges: Along these edges, the follower maintains a fixed distance from its predecessor along its local Y -axis.

ii. Graph Constraints: Each follower node must have an out-degree of at least 2, including at least one outgoing X^+ -edge and one outgoing Y -edge.

For example, Fig. 1 illustrates a diamond formation with four nodes (one leader and three followers). The DAG associated with this formation has the following edge subsets:

- X^+ -edges: $\{(F_1 \rightarrow L), (F_2 \rightarrow L), (F_3 \rightarrow F_2)\}$,
- Y -edges: $\{(F_1 \rightarrow L), (F_2 \rightarrow F_1), (F_3 \rightarrow F_1)\}$.

This configuration guarantees that every follower meets the minimum out-degree requirements.

C. String Stability

Following the definition in [20], string stability quantifies the ability of a follower to attenuate disturbances originating from the leader. Denote by \mathcal{S} the string stability gain, defined as the ratio of the disturbance amplitude at the follower to that at the leader. The formation is deemed string stable if $\mathcal{S} < 1$, which implies that perturbations diminish as they propagate along the formation. Furthermore, safe operation requires that the inter-agent distances remain within a prescribed range: above a minimum threshold to avoid collisions and below a maximum limit to preserve formation integrity.

In subsequent sections, Lyapunov functions and control barrier functions are employed to design a controller that simultaneously guarantees safety and string stability with formation tracking.

III. ESTIMATOR-BASED SAFETY CRITICAL CONTROLLER

In the absence of explicit communication, each agent must estimate the velocity components of its predecessor to achieve robust formation tracking. Fig. 3 provides a schematic of the estimator-based safety-critical control architecture. The following sections detail the design of the estimator, a rigorous stability analysis, and the integration of the estimator into the control law.

A. Estimator Design

Define the measurable quantities in the follower's local frame:

$$d_x = d \cos \theta, \quad d_y = d \sin \theta,$$

and let the true state vector associated with the predecessor be

$$x = [d_x, v_{1x}, d_y, v_{1y}]^T.$$

The estimator generates the corresponding state estimates

$$\hat{x} = [\hat{d}_x, \hat{v}_{1x}, \hat{d}_y, \hat{v}_{1y}]^T,$$

Let g_d , g_v , and p be positive constant gains. Assuming the follower has access to its own linear velocity v , angular velocity ω , and the relative measurements d and θ , the proposed estimator is given by

$$\begin{aligned} \dot{\hat{d}}_x &= \hat{v}_{1x} - v + d \omega \sin \theta + g_d \tilde{d}_x, \\ \dot{\hat{v}}_{1x} &= g_v \tilde{d}_x + \hat{v}_{1y} \omega + p \omega \tilde{d}_y, \\ \dot{\hat{d}}_y &= \hat{v}_{1y} - d \omega \cos \theta + g_d \tilde{d}_y, \\ \dot{\hat{v}}_{1y} &= g_v \tilde{d}_y - \hat{v}_{1x} \omega - p \omega \tilde{d}_x. \end{aligned} \quad (4)$$

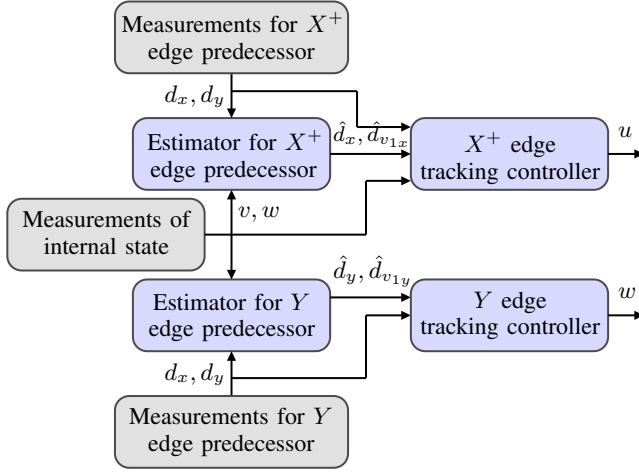


Fig. 3. Block diagram of the proposed estimator-integrated safety-critical control system, illustrating the interconnection of the estimator and controller modules within the decentralized formation control framework.

where the estimation errors are defined as

$$\tilde{e} = x - \hat{x} = [\tilde{d}_x, \tilde{v}_{1x}, \tilde{d}_y, \tilde{v}_{1y}]^T.$$

Using the estimates, the predecessor's heading and speed can be reconstructed as

$$\begin{aligned} \hat{\psi} &= \arctan\left(\frac{\hat{v}_{1y}}{\hat{v}_{1x}}\right), \\ \hat{v}_1 &= \sqrt{\hat{v}_{1x}^2 + \hat{v}_{1y}^2}. \end{aligned} \quad (5)$$

The error dynamics, derived from the difference between the true system dynamics (2) and estimator dynamics (4), can be expressed in compact form:

$$\dot{\tilde{e}} = \underbrace{\begin{bmatrix} g_d & 1 & 0 & 0 \\ g_v & 0 & p\omega & \omega \\ 0 & 0 & g_d & 1 \\ -p\omega & -\omega & g_v & 0 \end{bmatrix}}_{A(\omega)} \tilde{e} + \underbrace{\begin{bmatrix} 0 & 0 \\ -1 & 0 \\ 0 & 0 \\ 0 & -1 \end{bmatrix}}_B \begin{bmatrix} a_x \\ a_y \end{bmatrix}. \quad (6)$$

Here, the matrix $A(\omega)$ explicitly depends on the angular velocity ω , and the term involving a_x and a_y accounts for the influence of the predecessor's acceleration in the follower's frame.

The formulation in (6) provides a basis for a stability analysis of the estimator using Lyapunov techniques. In the following section, we leverage these dynamics along with control barrier functions to synthesize a safety-critical controller that ensures accurate formation tracking and collision avoidance.

B. Stability Analysis

To establish the convergence properties of the estimator, we analyze the stability of the error dynamics under three scenarios using appropriate Lyapunov function candidates. These scenarios are:

Case 1: Constant Predecessor Velocity. The predecessor maintains a constant linear velocity and zero angular velocity. This ideal case serves as a baseline, where exponential convergence of the estimation error is expected.

Case 2: Time-Varying Predecessor Velocity with Zero Angular Velocities. The predecessor's linear velocity varies with time

while both the predecessor's angular velocity (ω_1) and the follower's angular velocity (ω) are zero. Here, we prove that the estimation errors remain globally uniformly ultimately bounded.

Case 3: General Motion. The predecessor exhibits both time-varying linear velocity and nonzero angular velocity. In this most general scenario, we demonstrate that the estimator errors remain globally bounded.

Below, we detail the analysis for these cases.

Case 1. Constant Velocity: Assume that the predecessor's linear velocity is constant and $\omega_1 = 0$ (implying $\omega = 0$ in the estimator dynamics). Define the quadratic Lyapunov function candidate

$$V_1(\tilde{e}) = \tilde{e}^T P \tilde{e}, \quad P = P^T \succ 0, \quad (7)$$

where $\tilde{e} \in \mathbb{R}^4$ is the estimation error defined in (6). To ensure that \dot{V}_1 is negative definite, the matrix P is chosen to satisfy the continuous-time algebraic Riccati equation (CARE)

$$A^T P + P A + Q = 0, \quad Q = Q^T \succ 0, \quad (8)$$

with A being the state matrix in (6) evaluated at $\omega = 0$.

Lemma 1. *For a Hurwitz matrix A and any given $Q = Q^T \succ 0$, there exists a unique solution $P = P^T \succ 0$ to (8) [21].*

The lemma guarantees that if A is Hurwitz (i.e., all eigenvalues of A have negative real parts), then the Lyapunov function V_1 ensures exponential stability of the error dynamics. The Hurwitz condition imposes constraints on the estimator gains. In particular, the characteristic equation associated with A is

$$\omega^2(\lambda - g_d + p)^2 + (\lambda^2 - g_d\lambda - g_v)^2 = 0. \quad (9)$$

For all roots λ to have negative real parts, it is necessary that

$$g_d < 0, \quad \frac{-g_d^2}{4} \leq g_v < 0, \quad (10)$$

$$p = \frac{1}{2} \left(g_d + \sqrt{g_d^2 + 4g_v} \right). \quad (11)$$

Case 2. Time-Varying Linear Velocity with $\omega = \omega_1 = 0$: In this scenario, the error dynamics (6) reduce to

$$\dot{\tilde{e}} = \begin{bmatrix} g_d & 1 & 0 & 0 \\ g_v & 0 & 0 & 0 \\ 0 & 0 & g_d & 1 \\ 0 & 0 & g_v & 0 \end{bmatrix} \tilde{e} + \begin{bmatrix} 0 & 0 \\ -1 & 0 \\ 0 & 0 \\ 0 & -1 \end{bmatrix} a_e, \quad (12)$$

where $a_e = \begin{bmatrix} a_x \\ a_y \end{bmatrix}$ represents the acceleration terms in the follower's frame.

For the analysis along the follower's x -axis, define the Lyapunov candidate

$$V(\tilde{d}_x, \tilde{v}_x) = \frac{1}{2} \left((r \tilde{d}_x - \tilde{v}_x)^2 + |g_v| \tilde{d}_x^2 + \tilde{v}_x^2 \right), \quad (13)$$

where the scalar parameter $r = \frac{1}{2}(-g_d + \sqrt{g_d^2 + 4g_v})$. The gains g_d and g_v are chosen such that $r > 1$. Notably, r is a root of the characteristic equation $r^2 + r g_d - g_v = 0$, which is useful in subsequent derivation. It is immediate that $V(0, 0) = 0$ and $V(\tilde{d}_x, \tilde{v}_x) \geq 0$, confirming that V is a valid Lyapunov function.

Theorem 1: Under the error dynamics (12) and with the Lyapunov function (13), the estimation error $(\tilde{d}_x, \tilde{v}_x)$ is globally uniformly ultimately bounded (GUUB). Moreover, if the predecessor's velocity becomes constant (i.e., $a_x \equiv 0$), then the estimation error converges asymptotically to zero.

Proof. We analyze the stability properties of the estimator by examining the time derivative of the Lyapunov function V :

$$\begin{aligned}\dot{V} &= (r\tilde{d}_x - \tilde{v}_x)(rg_d\tilde{d}_x + r\tilde{v}_x - g_v\tilde{d}_x + a_x) \\ &\quad + |g_v|\tilde{d}_x(g_d\tilde{d}_x + \tilde{v}_x) + \tilde{v}_x(g_v\tilde{d}_x - a_x) \\ &= (r\tilde{d}_x - \tilde{v}_x)(-r^2\tilde{d}_x + r\tilde{v}_x + a_x) + |g_v|g_d\tilde{d}_x^2 - \tilde{v}_xa_x \\ &= -r(r\tilde{d}_x - \tilde{v}_x)^2 + (r\tilde{d}_x - \tilde{v}_x)a_x + |g_v|g_d\tilde{d}_x^2 - \tilde{v}_xa_x \\ &= -r(r\tilde{d}_x - \tilde{v}_x)^2 + 2(r\tilde{d}_x - \tilde{v}_x)a_x + |g_v|g_d\tilde{d}_x^2 - r\tilde{d}_xa_x \\ &= (1-r)(r\tilde{d}_x - \tilde{v}_x)^2 + (|g_v|g_d + \frac{r^2}{4})\tilde{d}_x^2 \\ &\quad - (r\tilde{d}_x - \tilde{v}_x - a_x)^2 - (\frac{r}{2}\tilde{d}_x - a_x)^2 + 2a_x^2\end{aligned}\quad (14)$$

Applying the physical constraint on the magnitude of acceleration, $|a_x| < a_{\max}$, we obtain:

$$\begin{aligned}\dot{V} &\leq (1-r)(r\tilde{d}_x - \tilde{v}_x)^2 + (|g_v|g_d + \frac{r^2}{4})\tilde{d}_x^2 \\ &\quad - (|r\tilde{d}_x - \tilde{v}_x| - a_{\max})^2 - (\frac{r}{2}\tilde{d}_x - a_{\max})^2 + 2a_{\max}^2\end{aligned}\quad (15)$$

Defining $c_i = 2a_{\max}^2$, and considering the expression for \dot{V} , we conclude $\dot{V} < 0$ (indicating stability) as long as one of the following conditions holds:

$$|\tilde{d}_x| > \epsilon_d \triangleq \min\left(\frac{2(\sqrt{c_i} + a_{\max})}{r}, \sqrt{\frac{c_i}{k_d}}\right) \quad (16)$$

where $k_d = -(|g_v|g_d + \frac{r^2}{4})$, or

$$|r\tilde{d}_x - \tilde{v}_x| > \epsilon_v \triangleq \min\left(\sqrt{c_i} + a_{\max}, \sqrt{\frac{c_i}{r-1}}\right) \quad (17)$$

where ϵ_d and ϵ_v represent bounds on the estimation errors in d_x and v_x respectively.

Invoking an extension of Lyapunov's theorem, we establish the estimator's global stability and the GUUB property of d_x and v_x . \square

The numerator of the error bounds depends on the system's maximum acceleration (a_{\max}), which is a physical constraint. The denominator, however, depends on the estimator gains. This indicates we can tune the estimator's behavior to achieve tighter error bounds and improve control performance.

A similar analysis, based on an analogous Lyapunov function, can be applied to the y -axis error dynamics to demonstrate the GUUB property for $(\tilde{d}_y, \tilde{v}_y)$ under time-varying acceleration with $\omega = 0$.

Case 3. Time-Varying Linear and Non-Zero Angular Velocity: We now extend the stability analysis to the general scenario in which the predecessor exhibits both a time-varying linear

velocity and a non-zero angular velocity. In this case, the estimator error dynamics can be written as

$$\dot{\tilde{e}} = \underbrace{\begin{bmatrix} g_d & 1 & 0 & 0 \\ g_v & 0 & 0 & 0 \\ 0 & 0 & g_d & 1 \\ 0 & 0 & g_v & 0 \end{bmatrix}}_{A_0} \tilde{e} + \underbrace{\begin{bmatrix} 0 & 0 \\ -1 & 0 \\ 0 & 0 \\ 0 & -1 \end{bmatrix}}_B \begin{bmatrix} a_x - p\omega\tilde{d}_y - \omega\tilde{v}_y \\ a_y + p\omega\tilde{d}_x + \omega\tilde{v}_x \end{bmatrix}, \quad (18)$$

where $\tilde{e} = [\tilde{d}_x \ \tilde{v}_x \ \tilde{d}_y \ \tilde{v}_y]^T$ denotes the estimation error vector. The terms involving ω account for the coupling introduced by the non-zero angular velocity.

To analyze the stability of (18), we adopt Lyapunov candidates analogous to those used in Case 2, defined separately for the x - and y -components:

$$V_1 = \frac{1}{2} \left((r\tilde{d}_x - \tilde{v}_x)^2 + |g_v|\tilde{d}_x^2 + \tilde{v}_x^2 \right), \quad (19)$$

$$V_2 = \frac{1}{2} \left((r\tilde{d}_y - \tilde{v}_y)^2 + |g_v|\tilde{d}_y^2 + \tilde{v}_y^2 \right), \quad (20)$$

$$V = V_1 + V_2. \quad (21)$$

Here, $r > 1$ is a design parameter to be determined.

Theorem 2: Under the estimator dynamics (18) and with the Lyapunov function V defined in (21), the estimation error \tilde{e} is globally uniformly ultimately bounded (GUUB). Moreover, when the predecessor's linear and angular velocities converge to constant values, the estimation error \tilde{e} converges asymptotically to zero.

Proof. Following a similar calculation to Theorem 1, we obtain expressions for the time derivatives of V_1 and V_2 :

$$\begin{aligned}\dot{V}_1 &= -r(r\tilde{d}_x - \tilde{v}_x)^2 + |g_v|g_d\tilde{d}_x^2 \\ &\quad + (r\tilde{d}_x - 2\tilde{v}_x)(a_x - p\omega\tilde{d}_y - \omega\tilde{v}_y)\end{aligned}\quad (22)$$

$$\begin{aligned}\dot{V}_2 &= -r(r\tilde{d}_y - \tilde{v}_y)^2 + |g_v|g_d\tilde{d}_y^2 \\ &\quad + (r\tilde{d}_y - 2\tilde{v}_y)(a_y + p\omega\tilde{d}_x + \omega\tilde{v}_x)\end{aligned}\quad (23)$$

Substituting $r = -2p$ into these expressions, we arrive at a simplified expression for the time derivative of the combined Lyapunov derivative, $\dot{V} = \dot{V}_1 + \dot{V}_2$:

$$\begin{aligned}\dot{V} &= -r(r\tilde{d}_x - \tilde{v}_x)^2 + |g_v|g_d(\tilde{d}_x^2 + \tilde{d}_y^2) - r(r\tilde{d}_y - \tilde{v}_y)^2 \\ &\quad + (r\tilde{d}_x - 2\tilde{v}_x)a_x + (r\tilde{d}_y - 2\tilde{v}_y)a_y \\ &= (1-r)((r\tilde{d}_x - \tilde{v}_x)^2 + (r\tilde{d}_y - \tilde{v}_y)^2) + k_d(\tilde{d}_x^2 + \tilde{d}_y^2) \\ &\quad - (r\tilde{d}_x - \tilde{v}_x - a_x)^2 - (\frac{r}{2}\tilde{d}_x - a_x)^2 + 2a_x^2 \\ &\quad - (r\tilde{d}_y - \tilde{v}_y - a_y)^2 - (\frac{r}{2}\tilde{d}_y - a_y)^2 + 2a_y^2\end{aligned}\quad (24)$$

Incorporating the physical constraint on the magnitude of the predecessor's acceleration $a_x^2 + a_y^2 < a_{\max}^2$, we complete the square to obtain an expression for \dot{V} .

$$\begin{aligned}\dot{V} &\leq (1-r)((r\tilde{d}_x - \tilde{v}_x)^2 + (r\tilde{d}_y - \tilde{v}_y)^2) + k_d(\tilde{d}_x^2 + \tilde{d}_y^2) \\ &\quad - (|r\tilde{d}_x - \tilde{v}_x| - a_{\max})^2 - (\frac{r}{2}\tilde{d}_x - a_{\max})^2 \\ &\quad - (|r\tilde{d}_y - \tilde{v}_y| - a_{\max})^2 - (\frac{r}{2}\tilde{d}_y - a_{\max})^2 + 2a_{\max}^2\end{aligned}\quad (25)$$

By carefully analyzing the form of \dot{V} , we derive conditions under which it is strictly negative. These conditions translate into bounds on the estimation errors \tilde{d}_x , \tilde{d}_y , \tilde{v}_x , and \tilde{v}_y , demonstrating the GUUB property of the estimator.

Exploiting the constraint $r^2 + rg_d - g_v = 0$ and the substitution $r = -2p$, we obtain an explicit relationship between the estimator gains g_d and g_v :

$$p = \frac{g_d}{3} \text{ and } g_v = \frac{-2g_d^2}{9} \quad (26)$$

This indicates that the estimator behavior can be tuned primarily through the choice of g_d . \square

Theorem 2 confirms two key points: (i) the state estimation process is independent of the robot's angular velocity (ω), and (ii) based on the derived relationships between the estimator gains, we can primarily tune the estimator's performance by adjusting the single parameter g_d . Importantly, the analysis shows that the estimator's performance is invariant with respect to the robot's own angular velocity, thus supporting robust state estimation regardless of rotational motion.

C. Safety-Critical Controller Design

Leveraging the estimator described in Section II-B, each agent computes state estimates of its predecessor(s) along both X^+ -edges and Y -edges as defined by the underlying DAG. In this section, we design a safety-critical tracking controller that utilizes these estimates to ensure that the follower maintains the prescribed inter-agent distances concurrently along the X^+ - and Y -axes.

To enforce safety along the X^+ -edge, we define the safety function

$$h_1(d_x, v) \triangleq d_x - d_s - Tv, \quad (27)$$

where d_x is the measured longitudinal distance (along the follower's x -axis) from the follower to its predecessor, $d_s > 0$ is the desired safe distance, v is the follower's linear velocity, and $T > 0$ is the prescribed time headway, which provides a buffer for reaction time and enhances string stability.

Accordingly, the safe set is defined as

$$\mathcal{C} \triangleq \{(d_x, v) \in \mathbb{R}^2 : h_1(d_x, v) \geq 0\}. \quad (28)$$

Definition 1. Let $h_1 : \mathbb{R}^2 \rightarrow \mathbb{R}$ be continuously differentiable. The set \mathcal{C} in (28) is forward invariant if there exists an extended class \mathcal{K} function [22] denoted by $\alpha : \mathbb{R}_+ \rightarrow \mathbb{R}_+$ such that for all (d_x, v)

$$\dot{h}_1(d_x, v) \geq -\alpha(h_1(d_x, v)). \quad (29)$$

To derive an explicit bound on the follower's acceleration that guarantees safety, we differentiate (27) with respect to time. Noting that

$$\dot{d}_x = v_{1x} + d_y \omega - v \quad \text{and} \quad \dot{v} = u,$$

we obtain

$$\dot{h}_1 = v_{1x} - v + d_y \omega - Tu. \quad (30)$$

Enforcing the CBF condition (29) yields

$$v_{1x} - v + d_y \omega - Tu \geq -\alpha(h_1), \quad (31)$$

or equivalently,

$$Tu \leq v_{1x} - v + d_y \omega + \alpha(h_1). \quad (32)$$

In practice, since the true value of v_{1x} is estimated as \hat{v}_{1x} with a bounded estimation error (upper bound $E_u > 0$), we conservatively write

$$Tu \leq \hat{v}_{1x} - E_u - v + d_y \omega + \alpha(h_1). \quad (33)$$

By introducing a nonnegative tuning parameter x_c , we transform the inequality into the following closed-form control law:

$$u = \kappa \left(\hat{v}_{1x} - E_u - x_c - v + d_y \omega + \alpha(h_1) \right), \quad (34)$$

where $\kappa \triangleq \frac{1}{T}$.

To ensure that the follower converges to the desired longitudinal position, we define the tracking error via the Lyapunov candidate

$$V_x \triangleq \frac{1}{2} \left(\hat{d}_x - d_x^* - Tv \right)^2, \quad (35)$$

where \hat{d}_x is the estimated longitudinal position and d_x^* is the desired position. Differentiating V_x with respect to time and substituting the control law (34) yields

$$\begin{aligned} \dot{V}_x &= \left(\hat{d}_x - d_x^* - Tv \right) \left(\hat{v}_{1x} - v + d_y \omega + g_d \tilde{d}_x - Tu \right) \\ &= \left(\hat{d}_x - d_x^* - Tv \right) \left(E_u + x_c - \alpha(h_1) + g_d \tilde{d}_x \right), \end{aligned} \quad (36)$$

where we have accounted for the estimation error in \hat{v}_{1x} by introducing the term E_u and \tilde{d}_x denotes the estimation error in d_x . Defining

$$\hat{h}_1 \triangleq \hat{d}_x - d_s - Tv \quad \text{and} \quad d_e^* \triangleq d_x^* - d_s,$$

the derivative can be recast as

$$\dot{V}_x = \left(\hat{h}_1 - d_e^* \right) \left(E_u + x_c - \alpha(\hat{h}_1 - \tilde{d}_x) + g_d \tilde{d}_x \right). \quad (37)$$

For analytical convenience, we select the extended class \mathcal{K} function

$$\alpha(h) = -g_d h,$$

which is valid since $g_d < 0$, ensuring that $\alpha(h) > 0$ for $h > 0$ and $\alpha(0) = 0$. With this choice, the time derivative simplifies to

$$\dot{V}_x = g_d \left(\hat{h}_1 - d_e^* \right)^2 + \left(\hat{h}_1 - d_e^* \right) \left(E_u + x_c + g_d d_e^* \right). \quad (38)$$

This expression will be instrumental in establishing the stability of the overall estimator-controller framework.

Similarly, to maintain a safe lateral separation along the Y -edge, we define the lateral safety function

$$h_2 \triangleq \frac{d_s}{|d_s|} (d_y - d_s), \quad (39)$$

where d_y represents the lateral distance from the Y -edge predecessor and $d_s \neq 0$ is the desired safe distance. The factor $\frac{d_s}{|d_s|}$ acts as a sign indicator to ensure that $h_2 > 0$ when the magnitude of the lateral separation exceeds the safety threshold, regardless of the sign of d_y .

Differentiating h_2 with respect to time gives

$$\begin{aligned}\dot{h}_2 &= \frac{d_s}{|d_s|} \dot{d}_y \\ &= \frac{d_s}{|d_s|} (v_{1y} - d_x \omega),\end{aligned}\quad (40)$$

where d_x is the longitudinal distance from the Y -edge predecessor (measured along the follower's X -axis).

Enforcing the CBF condition

$$\dot{h}_2 \geq -\alpha(h_2) \quad (41)$$

with the same extended class \mathcal{K} function $\alpha(h) = -g_d h$ (recall that $g_d < 0$ so that $\alpha(h) > 0$ for $h > 0$), we obtain

$$\frac{d_s}{|d_s|} (v_{1y} - d_x \omega) \geq g_d h_2. \quad (42)$$

Rearranging, this yields

$$\frac{d_s}{|d_s|} d_x \omega \leq \frac{d_s}{|d_s|} (v_{1y} - g_d (d_y - d_s)). \quad (43)$$

Accounting for the estimation error in v_{1y} (with an upper bound $E_\omega > 0$) by expressing $v_{1y} = \hat{v}_{1y} - E_\omega$, we can conservatively write

$$\frac{d_s}{|d_s|} d_x \omega \leq \frac{d_s}{|d_s|} (\hat{v}_{1y} - g_d (d_y - d_s)) - E_\omega. \quad (44)$$

Introducing a nonnegative tuning constant y_c , we transform the inequality into an equality to obtain the lateral control law:

$$\omega = \frac{\hat{v}_{1y} - g_d (d_y - d_s)}{d_x} - \frac{|d_s| (E_\omega + y_c)}{d_s d_x}. \quad (45)$$

To enforce convergence to the desired lateral position, we define the lateral tracking Lyapunov function

$$V_y \triangleq \frac{1}{2} (\hat{d}_y - d_y^*)^2, \quad (46)$$

where \hat{d}_y is the estimated lateral position and d_y^* is the desired lateral position. Differentiating V_y and substituting the control law (45) yields

$$\begin{aligned}\dot{V}_y &= (\hat{d}_y - d_y^*) \dot{\hat{d}}_y \\ &= (\hat{d}_y - d_y^*) (\hat{v}_{1y} - d_x \omega + g_d \tilde{d}_y) \\ &= (\hat{d}_y - d_y^*) \left(\frac{|d_s| (E_\omega + y_c)}{d_s} + g_d (d_y - d_s) + g_d \tilde{d}_y \right) \\ &= (\hat{d}_y - d_y^*) \left(\frac{|d_s| (E_\omega + y_c)}{d_s} + g_d (\hat{d}_y - d_s) \right) \\ &= g_d (\hat{d}_y - d_y^*)^2 \\ &\quad + (\hat{d}_y - d_y^*) \left(\frac{|d_s| (E_\omega + y_c)}{d_s} + g_d (d_y^* - d_s) \right).\end{aligned}\quad (47)$$

This final form of \dot{V}_y demonstrates a quadratic dependence on the lateral tracking error, a desirable property for establishing stability.

To ensure overall stability of the formation control scheme under constant predecessor velocities, we propose the composite Lyapunov function

$$V \triangleq V_x + V_y + \tilde{e}^T P \tilde{e}, \quad (48)$$

where V_x is defined in (35) and accounts for longitudinal tracking, V_y is defined in (46) and accounts for lateral tracking, and $\tilde{e}^T P \tilde{e}$ represents the estimation error term with $P = P^T \succ 0$ being the unique solution to the continuous algebraic Riccati equation

$$A^T P + P A + Q = 0,$$

where A is as given in (6) and $Q = Q^T \succ 0$.

This composite Lyapunov function will be used to prove the stability of the overall estimator-controller framework.

Theorem 3: Consider the composite Lyapunov function in (48), the estimator design in (4), and the control laws in (34) and (45). If the predecessor maintains a constant velocity (i.e., $a_x = a_y = 0$), then the longitudinal and lateral tracking errors converge asymptotically to zero. In particular, the follower's longitudinal distance converges to $d_x \rightarrow d_x^ + T v$ and its lateral distance converges to $d_y \rightarrow d_y^*$, provided that*

$$d_x^* \geq d_s - \frac{E_u}{g_d} \quad \text{and} \quad \begin{cases} d_y^* \geq d_s - \frac{E_\omega}{g_d} & \text{if } d_s > 0, \\ d_y^* \leq d_s + \frac{E_\omega}{g_d} & \text{if } d_s < 0, \end{cases} \quad (49)$$

ensuring that the safety margins are maintained in both directions.

Proof. Recall the composite Lyapunov function in (48). Differentiating V along the system trajectories yields

$$\begin{aligned}\dot{V} &= \dot{V}_x + \dot{V}_y + \tilde{e}^T (A^T P + P A) \tilde{e} \\ &= g_d (\hat{h}_1 - d_e^*)^2 + (\hat{h}_1 - d_e^*) (E_u + x_c + g_d d_e^*) \\ &\quad - \tilde{e}^T Q \tilde{e} + g_d (\hat{d}_y - d_y^*)^2 \\ &\quad + (\hat{d}_y - d_y^*) \left(\frac{|d_s| (E_\omega + y_c)}{d_s} + g_d (d_y^* - d_s) \right),\end{aligned}\quad (50)$$

where we define $d_e^* \triangleq d_x^* - d_s$, and $Q = Q^T \succ 0$ is the weighting matrix from the continuous-time algebraic Riccati equation.

By design, the tuning parameters $x_c \geq 0$ and $y_c \geq 0$ are selected to cancel the linear terms. Specifically, we choose

$$x_c = -g_d (d_x^* - d_s) - E_u, \quad y_c = \frac{|d_s|}{d_s} (-g_d (d_y^* - d_s)) - E_\omega.$$

Substituting these expressions into (50) eliminates the cross terms, and we obtain

$$\dot{V} = g_d (\hat{h}_1 - d_e^*)^2 - \tilde{e}^T Q \tilde{e} + g_d (\hat{d}_y - d_y^*)^2. \quad (51)$$

Since $g_d < 0$ and $Q \succ 0$, it follows that \dot{V} is negative definite. By Lyapunov's direct method, the overall closed-loop system is asymptotically stable. Hence, the longitudinal error $(\hat{h}_1 - d_e^*)$ and the lateral error $(\hat{d}_y - d_y^*)$ converge asymptotically to zero. This implies that the follower's distances converge to

$$d_x \rightarrow d_x^* + T v \quad \text{and} \quad d_y \rightarrow d_y^*.$$

The conditions in (49) ensure that the desired setpoints are compatible with the imposed safety margins. Thus, both the longitudinal and lateral safety distances are maintained. \square

We now extend our analysis to the case where the predecessor's velocity varies over time. To establish stability under these

conditions, we consider the following augmented Lyapunov candidate function:

$$V \triangleq V_x + V_y + V_1 + V_2, \quad (52)$$

where V_x and V_y are the tracking Lyapunov functions defined in (35) and (46), respectively, and V_1 and V_2 are the Lyapunov functions associated with the estimator dynamics given in (21).

Theorem 4: Under the control laws (34) and (45) and the estimator design in (4), the longitudinal and lateral distances converge to their desired values, namely

$$d_x \rightarrow d_x^* + T v \quad \text{and} \quad d_y \rightarrow d_y^*,$$

while all system states remain globally uniformly ultimately bounded. This holds provided that

$$d_x^* \geq d_s - \frac{E_u}{g_d} \quad \text{and} \quad \begin{cases} d_y^* \geq d_s - \frac{E_\omega}{g_d}, & \text{if } d_s > 0, \\ d_y^* \leq d_s + \frac{E_\omega}{g_d}, & \text{if } d_s < 0. \end{cases}$$

Proof. We begin with the augmented Lyapunov function (52). Detailed calculations, which combine the results from Theorems 2 and 3, lead to an upper bound on the time derivative \dot{V} of the form

$$\begin{aligned} \dot{V} \leq & (1-r) \left((r \tilde{d}_x - \tilde{v}_x)^2 + (r \tilde{d}_y - \tilde{v}_y)^2 \right) + k_d (\tilde{d}_x^2 + \tilde{d}_y^2) \\ & - \left(|r \tilde{d}_x - \tilde{v}_x| - a_{\max} \right)^2 - \left(\left| \frac{r}{2} \tilde{d}_x \right| - a_{\max} \right)^2 \\ & - \left(|r \tilde{d}_y - \tilde{v}_y| - a_{\max} \right)^2 - \left(\left| \frac{r}{2} \tilde{d}_y \right| - a_{\max} \right)^2 \\ & + g_d (\hat{h}_1 - d_e^*)^2 + g_d (\hat{d}_y - d_y^*)^2 + 2a_{\max}^2, \end{aligned}$$

where $c_i \triangleq 2a_{\max}^2$, $d_e^* \triangleq d_x^* - d_s$, and the remaining terms are as defined previously.

It follows that \dot{V} is strictly negative whenever either

$$|\hat{d}_x - d_x^* - T v| > \epsilon_x \triangleq \sqrt{\frac{c_i}{|g_d|}} \quad (53)$$

or

$$|\hat{d}_y - d_y^*| > \epsilon_y \triangleq \sqrt{\frac{c_i}{|g_d|}}, \quad (54)$$

which provide explicit bounds on the longitudinal and lateral tracking errors.

By applying the GUUB result for time-varying systems [22], we conclude that the entire system—including the estimator and the formation tracking states—is globally uniformly ultimately bounded. Concretely, our composite Lyapunov function remains strictly decreasing outside an arbitrarily small neighborhood, forcing all trajectories to remain within a bounded set for all time. Moreover, combining these bounds with those derived in the estimator analysis, we obtain explicit expressions for the allowable deviations:

$$|d_x - d_x^* - T v| < \epsilon_x + \epsilon_d, \quad (55)$$

$$|d_y - d_y^*| < \epsilon_y + \epsilon_d, \quad (56)$$

where ϵ_d denotes the bound on the estimation error.

Thus, under the conditions in (49), the desired safety margins in both the longitudinal and lateral directions are maintained, and all state variables remain GUUB. \square

The GUUB properties of the estimator, combined with the robust safety-critical controller design, ensure that the system accommodates sensor noise and model inaccuracies while preserving safety. Although the current analysis is based on a simplified dynamic model that neglects friction and inertia, the approach can be extended to more complex dynamics by incorporating the corresponding physical effects.

D. String Stability

In our safety-critical formation control framework, we leverage the results of Swaroop and Hedrick [23], which show that maintaining an inter-vehicular distance satisfying

$$d \geq d_r + T v,$$

where d_r is a reference distance, T is a time headway, and v is the vehicle velocity, is sufficient to attenuate disturbances in a leader-follower configuration. In essence, any controller that enforces this inequality will ensure string stability even in the absence of inter-vehicle communication.

The safety-critical function defined in (27) and the desired tracking distance along the X^+ -edge, as established in Theorems 3 and 4, inherently satisfy the condition

$$d_x \geq d_s + T v,$$

which is in line with the string stability criterion. Consequently, our controller achieves string stability by ensuring that disturbances originating from the leader are attenuated as they propagate through the formation. This property is maintained even when the system is subject to nonlinear disturbances affecting both inter-vehicular distances and vehicle velocities.

Thus, by integrating the string stability criterion with CBFs and Lyapunov-based stability analysis, our estimator-based controller guarantees safety, preserves string stability, and maintains accurate formation tracking in communication-deprived environments.

IV. RESULTS AND EVALUATION

This section comprehensively evaluates the proposed estimator and control law across various formation control scenarios. The accuracy and convergence of the estimator are assessed under different conditions with zero and non-zero angular velocity. The system's behavior in a basic formation scenario is examined through a simulation of a four-agent system arranged in a diamond formation (as illustrated in Fig. 1), with the leader maintaining a constant velocity. This simulation allows observation of how the agents coordinate their movements and maintain the desired formation while adhering to safety constraints. String stability, a critical factor in the robustness of multi-agent systems, is thoroughly analyzed by examining the propagation of disturbances through the formation. This analysis provides valuable insights into how well the follower agents can mitigate the effects of disturbances from the leader and ensure the formation's overall stability. The evaluation extends beyond simulations in Python by conducting experiments in the physics engine-based Gazebo simulation environment. A three-agent system arranged in a triangular formation is simulated, introducing realistic physics and sensor noise into

the scenario. This simulation offers a more comprehensive and practical assessment of the system's performance, as it is exposed to challenges typically encountered in real-world applications.

The continuous-time behavior of the system is simulated using a 4th-order Runge-Kutta method. In these simulations, the distance sensor data is generated by computing the state differences between agents. The following bounds are imposed on the agents:

$$v \leq 1 \text{ m/s}, \quad u \leq 0.5 \text{ m/s}^2, \quad \omega \leq 2 \text{ rad/s}.$$

The estimator gain is set to

$$g_d = -15,$$

with the remaining parameters computed as

$$g_v = -50, \quad p = -5, \quad r = 10, \quad T = 0.2 \text{ sec}, \quad k_d = 725.$$

The safety bounds are specified as $E_u = 1.4$ and $E_\omega = 1.4$. With these gains, the state matrix A (refer to (6)) is Hurwitz for $\omega = 0$, with eigenvalues $\{-5, -5, -10, -10\}$, confirming the stability of the estimator.

A. Estimator Analysis

This subsection evaluates the performance of the proposed estimator under varying operating conditions. A two-agent system is simulated in which both agents accelerate for 2 seconds to reach a constant linear velocity of 0.2 m/s. In this simulation, Agent 1 maintains a constant angular velocity of 0.2 rad/s, whereas Agent 2 exhibits zero angular velocity. This experimental setup is used to investigate three distinct scenarios: a) estimating the state of the accelerating agent while accelerating, in which Agent 1 estimates the state of Agent 2 during the initial acceleration phase (0-2 seconds); b) estimating the state of an agent with constant linear velocity while moving with non-zero angular velocity, in which Agent 1 estimates the state of Agent 2 after the 2-sec acceleration phase, where Agent 2 is moving at a constant velocity while Agent 1 maintains its angular velocity; and c) estimating the state of an agent with non-zero angular velocity while moving with zero angular velocity, in which Agent 2 estimates the state of Agent 1 after the 2-sec acceleration phase, where Agent 1 is moving at a constant velocity with non-zero angular velocity while Agent 2 remains stationary in terms of angular motion.

For scenario (a), during the first 2 seconds both agents accelerate at 0.2 m/s^2 . Consistent with the analysis presented in Case 3 of Section III-B, the estimator is expected to exhibit GUUB behavior. The theoretical error bounds for the position and velocity are approximately $\pm\sqrt{c_i/k_d} \approx \pm 0.026 \text{ m}$ and $\pm\left(|r\tilde{d}_x| + \sqrt{c_i/(r-1)}\right) \approx 0.497 \text{ m/s}$, respectively. Numerical simulation results in Fig. 4 show that the position error converges to about 0.004 m and the velocity error to about 0.06 m/s, both well within the expected bounds.

In scenario (b), after the acceleration phase, Agent 2 moves at a constant velocity while Agent 1 maintains its angular motion. Since the estimator's convergence is theoretically independent of the observer's angular velocity, the estimation errors are anticipated to approach zero. Simulation results in Fig. 4

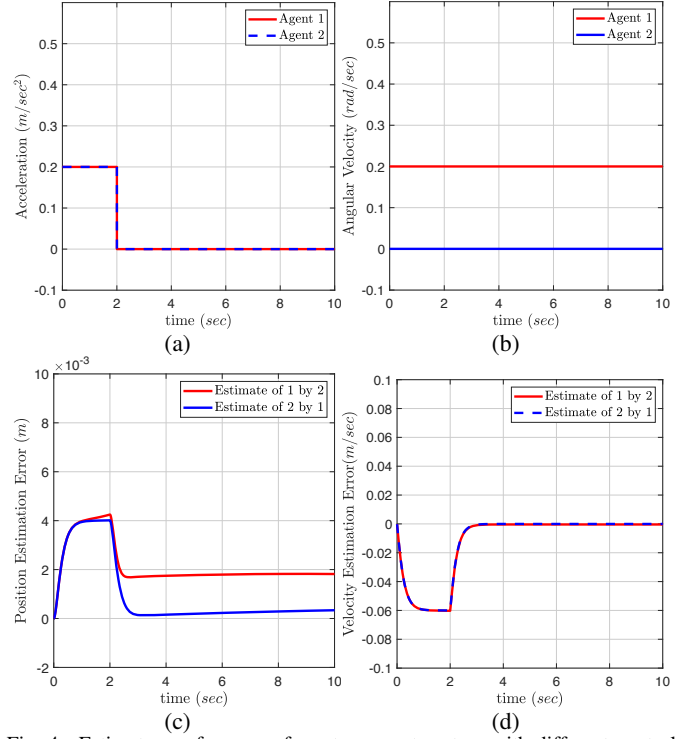


Fig. 4. Estimator performance for a two-agent system with different control profiles: (a) Linear acceleration profiles; (b) Angular velocities; (c) Position estimation errors; (d) Velocity estimation errors.

confirm this behavior, with the distance error converging to approximately 0.0003 m and the velocity error to roughly 0.00004 m/s.

In scenario (c), Agent 1 continues with constant linear and angular velocity, while Agent 2 remains with zero angular motion. Here, the estimator effectively interprets the angular motion as an additional acceleration term, computed as $a = u + v\omega = 0.08 \text{ m/s}^2$. Accordingly, the estimation errors are expected to remain GUUB with bounds similar to those in scenario (a). The simulation results in Fig. 4 corroborate this, showing convergence of the distance error to approximately 0.0018 m and the velocity error to about 0.0004 m/s.

B. Formation Control with Constant Leader Velocity

This section evaluates the proposed control framework under a constant leader velocity scenario. The leader agent accelerates to a fixed linear velocity while maintaining a constant angular velocity of $\omega = 0.5 \text{ rad/s}$, thereby steering along a circular trajectory—a common benchmark in formation control studies. Due to the non-zero angular velocity, both acceleration components a_x and a_y are non-zero, situating this scenario within the time-varying stability analysis of *Theorem 4*.

Figures 5(a), (b), and (c) display the linear velocity, acceleration, and angular velocity profiles for each agent throughout the experiment. The results indicate rapid convergence to a circular formation that closely tracks the leader's trajectory. In particular, the angular velocities of the follower agents converge to that of the leader, and their linear velocities adjust according to their respective circular motion radii. This coordinated behavior is achieved entirely through the proposed estimator-controller framework without any modifications to the control law.

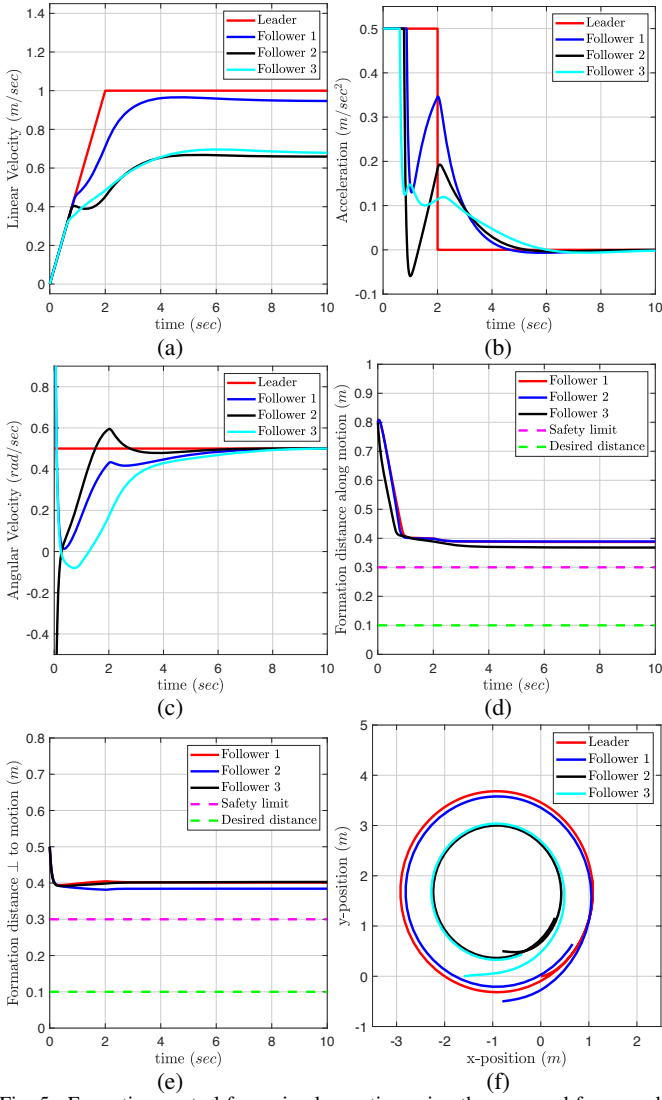


Fig. 5. Formation control for a circular motion using the proposed framework: (a) Linear velocity profiles; (b) Acceleration profiles; (c) Angular velocities; (d) Distances maintained along the motion; (e) Position estimation errors; (f) Distance perpendicular to the motion, and (g) Overall motion of the formation.

The safety region for each agent is defined as 0.3 m, with a desired separation of 0.1 m between followers. Figures 5(d) and (e) illustrate the evolution of the safety control barrier functions along and perpendicular to the agents' motion, respectively. Despite the desired separation falling within what might conventionally be considered an unsafe region, the agents consistently maintain a conservative minimum distance as prescribed by the safety constraints. Finally, Fig. 5(f) visually depicts the overall formation motion during the experiment.

A supplementary video demonstrating the circular formation scenario in Fig. 5 is provided alongside this paper.

C. String Stability Performance

String stability is a critical performance metric for leader-follower systems. It ensures that disturbances, such as sudden braking or acceleration, do not amplify as they propagate from the leader to the followers, thereby reducing the risk of collisions. In a string-stable formation control design, the amplitude of sinusoidal velocity disturbances should decrease

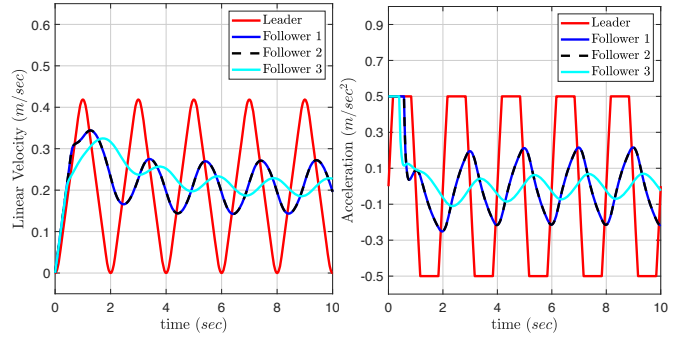


Fig. 6. Disturbance attenuation in linear velocity and acceleration for a 4-agent diamond formation control. Left: linear velocity disturbance of 0.415 m/s. Right: acceleration disturbance of 1.0 m/s².

along the formation. Fig. 6 illustrates the performance of the proposed controller in maintaining string stability for the considered formation.

In this experiment, the leader's velocity underwent a disturbance with an amplitude of 0.415 m/s. As the disturbance propagated through the formation, the resulting amplitudes diminished to 0.12 m/s for both follower 1 and follower 2, and further to 0.035 m/s for follower 3, as shown in Fig. 6(a). Similarly, when an acceleration disturbance of 1.0 m/s² was introduced, the proposed framework yielded acceleration responses of 0.434 m/s² for both follower 1 and follower 2, and 0.14 m/s² for follower 3, as shown in Fig. 6(b). Notably, the overlapping profiles of follower 1 and follower 2 are attributed to their identical state evolution and pursuit of the same predecessor.

The quantitative analysis reveals an average string stability gain (S) of 0.29. The observed reduction in disturbance amplitude along the platoon, together with $S < 1$, confirms that the proposed control law ensures string stability.

A video illustrating the oscillatory velocity disturbance experiments in Fig. 6 can be found in the supplementary video submitted with the paper.

D. Physics Engine-Based Experiments

To assess the feasibility and effectiveness of the proposed estimation-based controller in realistic scenarios, we implement the framework within the Gazebo simulation environment. In this experiment, a leader agent follows a time-varying trajectory within a simulated warehouse while two follower agents maintain a triangular formation with respect to the leader. Turtlebot3 models are employed to emulate the robotic agents. Key parameters for robot motion are set as follows: maximum linear velocity of 0.3 m/s, maximum angular velocity of 1.0 rad/s, and maximum acceleration of 1.0 m/s². Figure 7 shows a snapshot of the simulated warehouse environment.

A three-agent cluster operates without inter-vehicle communication. In this configuration, the leader exhibits variable velocity, and the follower agents maintain formation using the proposed controller. Initially, follower 1 and follower 2 are positioned at coordinates $(-0.5, -0.4)$ and $(-0.5, 0.4)$, respectively, relative to the leader. Emulated distance sensors provide measurements based on state differences between the agents. The estimator and controller are configured with parameters $g_d = -6$, $g_v = -8$, $p = -2$, $E_\omega = 0.4$ m-rad/s, $E_u = 0.4$ m/s, and

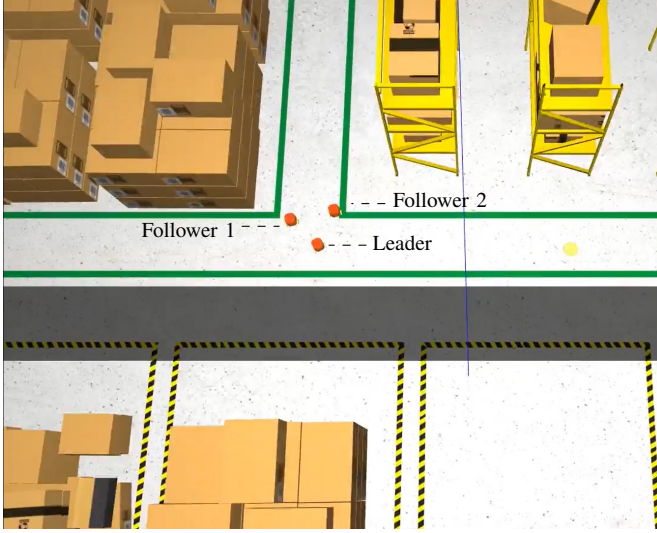


Fig. 7. Snapshot of the warehouse environment in Gazebo with three Turtlebot3 in a triangular formation.

$T = 0.2$ sec. Under these settings, the state matrix A (evaluated at $\omega = 0$) has eigenvalues $[-2, -2, -4, -4]$, which confirms its Hurwitz property and ensures estimator stability. Safety constraints are set to maintain a minimum distance of 0.2 m in all directions. In the formation, follower 1 and follower 2 track the leader along both the X^+ and Y edges. Their formation parameters are configured such that follower 1 maintains 0.4 m longitudinally and 0.3 m laterally, while follower 2 maintains 0.4 m longitudinally and -0.3 m laterally from the leader.

The leader agent's time-varying trajectory is determined by the angular velocity and acceleration curves shown in Fig. 8(a) and (b). These plots indicate that the proposed controller effectively generates the necessary acceleration and angular velocity commands to maintain the desired triangular formation. This is further supported by Fig. 8(c), which illustrates the evolution of the agents' linear velocities. When the leader operates with zero angular velocity, the linear velocities of both follower agents converge to that of the leader. Conversely, when the leader rotates about a center of rotation, the follower closer to the center reduces its speed, while the follower farther away increases its speed to preserve formation integrity. Notably, the angular velocities of all agents remain synchronized, as demonstrated in Fig. 8(a).

Figures 8(d) and (e) illustrate that the formation distances converge to their desired values when the leader's acceleration and angular velocity are zero. In scenarios with non-zero angular velocity, deviations between the actual formation distances and the desired distances remain bounded within 0.02 m along the direction of motion and 0.005 m in the perpendicular direction. Importantly, both follower agents consistently adhere to the predefined safety limits throughout the experiment. Finally, Fig. 8(f) visually represents the trajectories of the leader and follower agents.

The stability of the estimator within the Gazebo environment is critical for achieving optimal performance of the proposed framework. Fig. 9 illustrates the estimation errors in both the position and velocity of the leader as measured by the follower agents. As the followers track the leader, the estimation errors

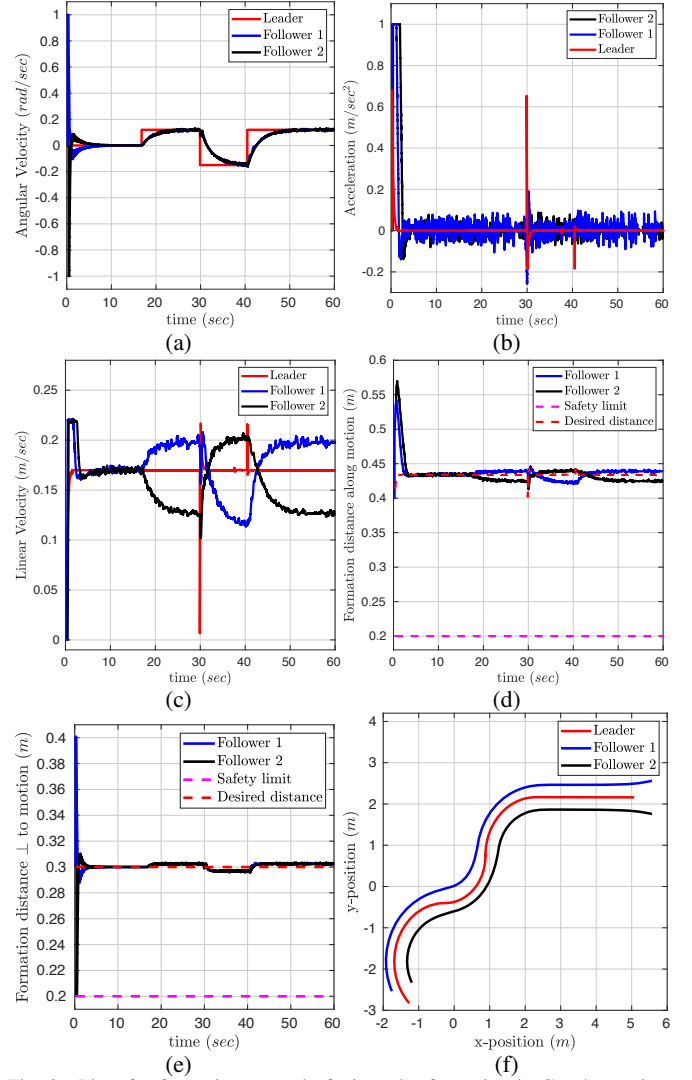


Fig. 8. Plots for formation control of triangular formation in Gazebo environment using the proposed framework: (a) Angular Velocity, (b) Acceleration, (c) Linear Velocity, (d) Distance along the motion, (e) Distance perpendicular to the motion, and (f) Overall motion of the formation.

are maintained at low levels; specifically, when the leader operates with zero angular velocity, the position estimation error remains below 0.002 m. For scenarios with non-zero leader angular velocity, the position estimation errors for both followers are bounded within 0.004 m. Moreover, the velocity estimation errors for both follower agents are kept below 0.006 m/s, which underscores the estimator's robustness in the presence of noise in real-world environments.

Videos of the experiment presented in this section, including a video of the Gazebo-based triangular formation experiments, can be found in the accompanying video for the article, available at:

<https://vimeo.com/1075016147/41612f2f8c>

The results obtained from the Gazebo simulation experiments substantiate the applicability and effectiveness of the proposed controller in realistic scenarios. Overall, the comprehensive evaluation demonstrates that the proposed framework maintains safety-critical performance while achieving the desired formation control.

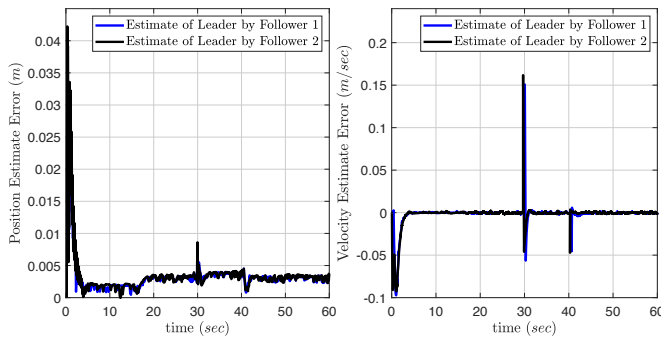


Fig. 9. Leader's position (left) and velocity (right) estimation error when estimated by follower agents.

V. CONCLUSIONS AND FUTURE WORK

In this paper, we have addressed the critical problem of ensuring stable, robust, and safe formation control for non-holonomic multi-agent systems operating in environments characterized by severe communication limitations. A novel decentralized estimator-based safety-critical controller framework has been introduced, designed to guarantee formation integrity, collision avoidance, and disturbance attenuation without relying on explicit inter-agent communication.

Our approach incorporates a robust state estimator specifically tailored to non-holonomic robotic systems, capable of reliably estimating neighboring agents' velocity vectors and orientations even under time-varying velocities and angular motions. Using Lyapunov-based stability analysis, we have proven the global asymptotic stability of estimation errors under constant velocity conditions and their global uniform ultimate boundedness under more general time-varying scenarios.

The proposed safety-critical controller effectively integrates CBFs with the estimator to ensure collision avoidance and maintain safe inter-agent distances at all times. Additionally, we have introduced and validated the concept of string stability within the leader-follower formation framework, demonstrating significant attenuation of disturbances as they propagate throughout the formation.

Extensive numerical simulations, complemented by realistic Gazebo-based experiments involving sensor noise and physical constraints, validate the practical applicability, robustness, and effectiveness of our proposed method. The experimental results highlight the controller's ability to maintain stringent safety margins while reliably tracking complex formations under realistic operational conditions.

This research advances the field of formation control, particularly for safety-critical applications where communication constraints are prevalent. Future work will explore dynamic formation reconfiguration under safety-critical constraints, extend our methodology to more complex robotic platforms and heterogeneous multi-robot systems, and integrate additional functionalities such as obstacle avoidance and environmental interaction, to further enhance the framework's applicability to real-world scenarios.

REFERENCES

[1] R. N. Darmanin and M. K. Bugeja, "A review on multi-robot systems categorised by application domain," in *2017 25th Mediterranean Conference on Control and Automation (MED)*, 2017, pp. 701–706.

[2] K.-K. Oh, M.-C. Park, and H.-S. Ahn, "A survey of multi-agent formation control," *Automatica*, vol. 53, pp. 424–440, 2015.

[3] J. Lin, Y. Wang, Z. Miao, Q. Lin, G. Hu, and R. Fierro, "Robust linear-velocity-free formation tracking of multiple quadrotors with unknown disturbances," *IEEE Transactions on Control of Network Systems*, vol. 10, no. 4, pp. 1757–1769, 2023.

[4] P. Aditya, E. Apriliani, G. Zhai, and D. K. Arif, "Formation control of multi-robot motion systems and state estimation using extended kalman filter," in *2019 International Conference on Electrical Engineering and Informatics (ICEEI)*. IEEE, 2019, pp. 99–104.

[5] S. Moorthy and Y. H. Joo, "Formation control and tracking of mobile robots using distributed estimators and a biologically inspired approach," *Journal of Electrical Engineering & Technology*, vol. 18, no. 3, pp. 2231–2244, 2023.

[6] S. Zhu, K. Lv, Z. Yang, C. Chen, and X. Guan, "Bearing-based formation tracking control of nonholonomic mobile agents with a persistently exciting leader," *IEEE Transactions on Control of Network Systems*, vol. 11, no. 1, pp. 307–318, 2024.

[7] J. Zhao, K. Zhu, H. Hu, X. Yu, X. Li, and H. Wang, "Formation control of networked mobile robots with unknown reference orientation," *IEEE/ASME Transactions on Mechatronics*, vol. 28, no. 4, 2023.

[8] A. D. Ames, S. Coogan, M. Egerstedt, G. Notomista, K. Sreenath, and P. Tabuada, "Control barrier functions: Theory and applications," in *2019 18th European Control Conference (ECC)*, 2019, pp. 3420–3431.

[9] B. A. Butler, C. H. Leung, and P. E. Paré, "Collaborative safe formation control for coupled multi-agent systems," *arXiv preprint arXiv:2311.11156*, 2023.

[10] A. Rai and S. Mou, "Safe region multi-agent formation control with velocity tracking," *Systems & Control Letters*, vol. 186, p. 105776, 2024.

[11] B. Yan, P. Shi, C. P. Lim, Y. Sun, and R. K. Agarwal, "Security and safety-critical learning-based collaborative control for multiagent systems," *IEEE Transactions on Neural Networks and Learning Systems*, pp. 1–12, 2024.

[12] Y. Sun, D. Wu, L. Gao, Y. Gao, Y. Pan, and N. Ding, "Safety-critical control and path following by formations of agents with control barrier functions using distributed model predictive control," in *2023 35th Chinese Control and Decision Conference (CCDC)*, 2023.

[13] R. Rahimi, F. Abdollahi, and K. Naqshi, "Time-varying formation control of a collaborative heterogeneous multi agent system," *Robotics and autonomous systems*, vol. 62, no. 12, pp. 1799–1805, 2014.

[14] V. P. Tran, M. Garratt, and I. R. Petersen, "Switching time-invariant formation control of a collaborative multi-agent system using negative imaginary systems theory," *Control Engineering Practice*, vol. 95, p. 104245, Feb. 2020.

[15] H. Li, J. Hu, Q. Zhou, and B. K. Ghosh, "Safe formation control of multiple unmanned aerial vehicles: control design and safety-stability analysis," *Control Theory and Technology*, pp. 1–13, 2024.

[16] X. Liang, H. Wang, Y.-H. Liu, Z. Liu, and W. Chen, "Leader-following formation control of nonholonomic mobile robots with velocity observers," *IEEE/ASME Transactions on Mechatronics*, vol. 25, no. 4, pp. 1747–1755, 2020.

[17] Y. Hong, G. Chen, and L. Bushnell, "Distributed observers design for leader-following control of multi-agent networks (extended version)," *arXiv preprint arXiv:1801.00258*, 2017.

[18] L. Wang, J. Xi, M. He, and G. Liu, "Robust time-varying formation design for multiagent systems with disturbances: Extended-state-observer method," *International Journal of Robust and Nonlinear Control*, vol. 30, no. 7, p. 2796–2808, Mar. 2020.

[19] V. Bohara and S. Farzan, "Adaptive estimation-based safety-critical cruise control of vehicular platoons," *IEEE Transactions on Vehicular Technology*, pp. 1–13, 2024.

[20] G. Orosz, "Connected cruise control: modelling, delay effects, and nonlinear behaviour," *Vehicle System Dynamics*, vol. 54, no. 8, pp. 1147–1176, 2016.

[21] P. L. L. Rodman, *Algebraic Riccati equations*, 2nd ed. Oxford University Press, 1995.

[22] H. K. Khalil, *Nonlinear systems*, 2nd ed. Upper Saddle River, NJ 07458: Prentice-Hall, 2011.

[23] D. Swaroop, J. Hedrick, C. C. Chien, and P. Ioannou, "A comparison of spacing and headway control laws for automatically controlled vehicles1," *Vehicle System Dynamics*, vol. 23, no. 1, pp. 597–625, 1994.